

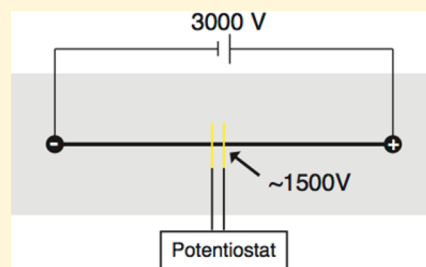
Microchannel Voltammetry in the Presence of Large External Voltages and Electric Fields

Lawrence P. Zaino, III,[†] William R. A. Wichert,[†] Garrison M. Crouch,[‡] and Paul W. Bohn^{*,†,‡}

[†]Department of Chemistry and Biochemistry, University of Notre Dame, Notre Dame, Indiana 46556, United States

[‡]Department of Chemical and Biomolecular Engineering, University of Notre Dame, Notre Dame, Indiana 46556, United States

ABSTRACT: The ability to perform electrochemistry in the presence of large voltages and electric field magnitudes without concern for the local potential has many possible applications in micro/nanofluidic assays and in capillary electrophoresis. Traditionally, electrochemistry in the presence of significant external electric fields has been dominated by end-channel detection for capillary and microchip electrophoresis detection. We describe novel instrumentation for potentiostatically controlled voltammetry that can be applied in the presence of high external voltages and electric fields. Cyclic voltammetry is demonstrated without significant shifts in the half-wave potential at working electrodes at local potentials of up to ~ 1500 V and field strengths of up to 3000 V/cm, using a standard Ag/AgCl reference electrode.



In the past decade, lab-on-a-chip (LOC) devices have rapidly evolved to demonstrate a multitude of analytical applications,^{1–3} and there is great interest in developing electrochemical techniques in both micro- and nanofluidic LOC devices.^{4,5} While pressure-driven flow is suitable for microfluidic devices in general, both microchip electrophoresis and devices with smaller dimensions (nanofluidics) require that pressure-driven flow be replaced by electrokinetic flow.^{6,7} The Hagen–Poiseuille equation dictates that the pressure needed to drive laminar flow scales like d^{-4} where d is the channel diameter, meaning that the pressure needed to drive flow becomes excessively large for many nanofluidic applications.⁸ Utilizing electrokinetic flow to manipulate solutions in nanochannel-based devices overcomes this problem. In addition, electro-osmotic flow is required intrinsically in microchip electrophoresis.^{7,9–11} However, integrating electrochemical detection strategies with the large external electric fields, $E \sim 10^3$ V cm⁻¹, needed for electrokinetic flow creates a number of issues, including solvent electrolysis, electrode dissolution, electrode instability, and damage to the potentiostat used to control the voltammetry.

One common approach to performing electrochemical measurements in large electric fields is to utilize bipolar electrodes (BPEs), i.e., electrically floating metal electrodes placed in the high-field environment, which drive electrochemical reactions based on the local potential difference between the electrode and solution. BPEs have been used for redox reactions as diverse as electrogenerated chemiluminescence and silver dissolution^{12–14} and have been used for applications like catalyst evaluation and concentration enrichment.^{15,16} Another structure-based strategy to couple electrochemistry with electrokinetic flow involves nanostructured solid-state architectures with arrays of nanocapillaries presenting embedded annular electrodes. These embedded annular nanoband electrode arrays achieve high fields at low voltages by

placing the working electrode a few μm from the counter electrode and, thus, support electrokinetically driven enhanced mass transport for electrochemical processing.^{17–19}

Lunte, Martin, Wightman, and others have pioneered a variety of strategies for in-channel electrochemical detection at high fields, for example, in microchip capillary electrophoresis applications. These include decoupling the electric field,^{20,21} dual-channel detection,²² and the development of isolated potentiostats.^{23,24} Previous iterations of isolated potentiostats have allowed in-channel detection in external electric fields by placing the working electrode (WE) in-channel, while the reference (RE) and counter (CE) electrodes are placed in a field-free volume, for example, in the buffer well at ground potential. While this works very well and is straightforward to fabricate, it limits the placement of the WE, because of iR -derived shifts in the actual potential.

$$E_{\text{actual}} = E_{\text{applied}} - iR \quad (1)$$

As the WE is moved further into the channel, the iR drop increases, causing large shifts in the actual potential at the WE compared to the nominal applied potential.^{25–27} This presents unique challenges for designing electrochemical devices, which incorporate electrokinetic flow. Decoupling the WE from the field in the microchannel greatly mitigates problems with iR drop and voltage shifts but at the expense of increased dead volume and degraded peak shapes. In addition, some previous approaches have grounded the RE, but this would clearly present problems if the RE is placed in the middle of a channel at high voltage.

Received: January 29, 2016

Accepted: March 25, 2016

Published: April 5, 2016

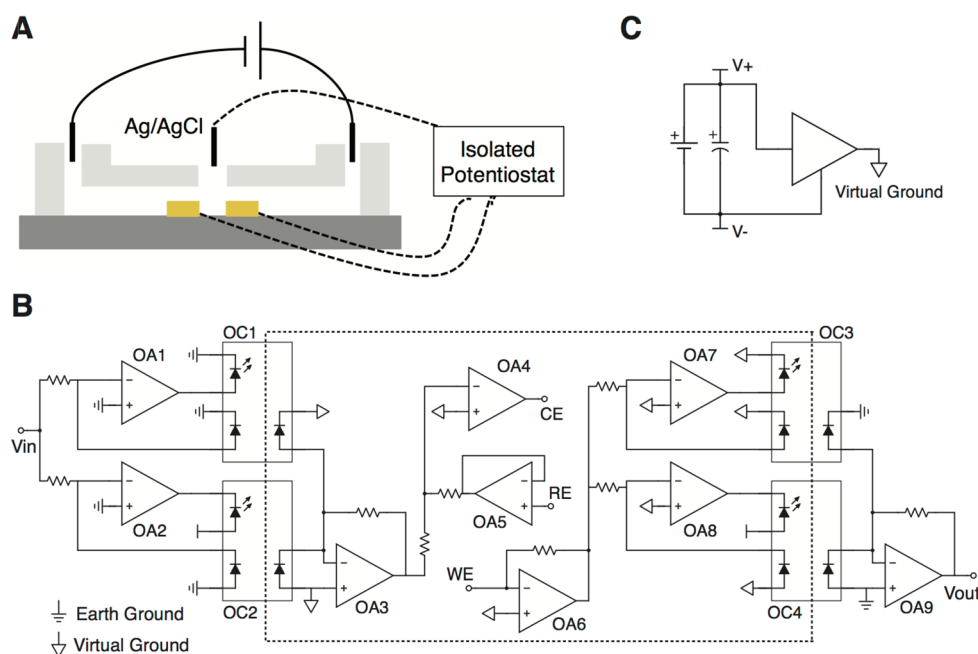


Figure 1. (A) Schematic illustration of the positioning of the working and counter electrodes relative to the electrified channel. (B) Circuit diagram of the optically isolated potentiostat. The components in the dashed box, OA3-8, are referenced to a virtual ground that can be set as desired and powered by a battery driven supply, based on a TLE 2426, shown in (C). The small rectangular boxes straddling the dashed rectangle represent four integrated optocouplers, OC1-4.

Ideally, one would like to perform voltammetry, as opposed to measurements at a single potential, in LOC devices and to do it independent of local potential or field strength, without shifting the observed potential of the voltammetric features. Approaches to this ideal have been achieved in certain special cases. For example, midchannel detection has been demonstrated at field strengths up to 400 V cm^{-1} by incorporating a polyelectrolyte gel salt bridge into a microfluidic device to separate the WE in the channel from the RE and CE.²²

Here, we describe instrumentation for integrating a three electrode cell into external electric fields regardless of location in the channel. This is accomplished through two advances: (1) a custom potentiostat, which allows the WE and CE to be placed at arbitrary locations directly in the external electric field, regardless of local potential and field strength, and (2) placing the RE just above the in-channel WE/CE pair with electrical communication established through a small access hole. We show that the custom potentiostat circuitry is capable of monitoring faradaic electron transfer at local potentials up to 1500 V and field strengths of 3000 V cm^{-1} .

EXPERIMENTAL SECTION

Reagents and Materials. Potassium ferricyanide (Fischer) and sodium phosphate (monobasic and dibasic, Sigma-Aldrich) were purchased and used as received. Deionized (DI) water ($R \sim 18 \text{ M}\Omega \text{ cm}$) from a milli-Q Gradient water purification system (Millipore) was used to prepare all solutions. Rapid prototyping was performed using *p*-type (100) Si wafers and SU-8 photoresist (MicroChem). Poly(dimethylsiloxane) (Sylgard 184, Dow Corning) was used to create microchannels. Electrodes were patterned on glass slides using S1813 (MicroChem) and AZ917-MIF developer (AZ Electronic Materials).

Fabrication. Metal electrodes were patterned by photolithography on glass slides. After photoresist development, an

electron beam evaporator was then used to deposit Ti and Au at a thickness of 5–10 and 150 nm, respectively. The WE and CE were 50 and $100 \mu\text{m}$ wide, respectively, and separated by $200 \mu\text{m}$. Microchannels were fabricated by first creating a master mold using Si wafers and SU-8. PDMS was then poured over the master, cured at $75 \text{ }^\circ\text{C}$, and placed onto the wafer to produce 2.4 cm long microchannels of $100 \mu\text{m}$ width and height. A 0.75 mm diameter punch was used to create an access hole for the Ag/AgCl reference electrode (RE). Oxygen plasma sealing was used to bind the PDMS to the wafer.

Optically Isolated Potentiostat. The isolated potentiostat was constructed starting from a traditional potentiostat design.²⁸ Bipolar optical isolation circuitry was built using HCNR200 optical couplers (Avago Technologies) using a dual optocoupler design according to manufacturers guidelines. The potentiostat and isolation circuitries were built using LT1097 operational amplifiers (Linear Technology). The isolated components of the instrument were battery powered using a TLE2426 rail-splitter with a virtual ground. The circuit components were not optimized for low noise measurements. Nonisolated components were powered using a $\pm 15 \text{ V DC}$ power supply. The magnitude, scan rate, and limits of triangular waveform were set using a custom LabView program. Data acquisition was also performed using LabView (2014, National Instruments). A data acquisition (DAQ) card (PCIe-6361, National Instruments) capable of both signal generation and measurement was used to interface between the isolated potentiostat and LabView. A data acquisition rate of 60 Hz was used. The external electric field was applied using 0.25 mm diameter Pt electrodes with a high voltage power supply (Bertan, 602c-30P). The experimental configuration and circuits are shown in Figure 1.

RESULTS AND DISCUSSION

Instrument Design Considerations. Traditional potentiostats can not be used to conduct electrochemistry at high voltage due to solvent electrolysis, electrode degradation, and possible instrument damage, all driven by the large voltage difference between the solution environment and the potentiostat components, which are typically referenced to earth ground. The potentiostat design described here for high-voltage/high-field voltammetry experiments is based on a traditional configuration but includes important modifications in order to allow electrochemical measurements at high voltage. In particular, the current follower circuit, which is used to measure the current through the WE in traditional potentiostat designs, is referenced to virtual earth ground by the operational amplifier (op-amp), OA6. Thus, if a large positive voltage is applied across a fluidic channel, any WE in the fluidic channel with a small applied potential ($|E_{WE}| < 1$ V) will experience a negative voltage offset in relation to the solvent and, thus, will function as a cathode, passing large ohmic currents. Under these conditions, the overpotential for water electrolysis could easily exceed 100 V, which would cause significant gas formation and likely destroy the electrode. Thus, in order to function at high voltage, the potentiostat circuitry must be designed to prevent solvent electrolysis and electrode degradation, while allowing faradaic electron transfer. In addition, as is typical in most LOC devices, we utilize thin film electrodes, which are especially susceptible to damage when large currents are passed through them. In order to prevent solvent electrolysis and possible damaging effects to the electrodes or instrument, the inverting inputs of both the control amplifier, OA4, and current follower, OA6, in Figure 1B have to be addressed.

The solution we have developed is to allow the inverting inputs of the op-amps constituting the WE current follower, OA6, and CE control amplifier, OA4, to float to the local potential of the electrified fluid. The simplest way to allow the components, OA6 and OA4, to float to the local potential is through a battery-based power supply illustrated in Figure 1C, rather than using a traditional power supply referenced to earth ground. A battery-based powered supply provides the offset isolation required to protect the potentiostat circuitry. In this case, a rail-splitter circuit was used in conjunction with a 9 V battery to power the potentiostat. This custom power supply provides ca. +4.5 and -4.5 V with respect to virtual ground, which is equivalent to the local potential in the electrified fluid. The virtual ground of the supply is equal to the local potential, because the negative-feedback loop of the op-amp equalizes the voltage of the inverting and noninverting leads, while the virtual ground floats to the local potential of the electrodes. For example, when the electrodes are at a local potential of ~ 50 V, the absolute potential of the virtual ground of the power supply is ~ 50 V with respect to earth ground. The rail-splitter circuit supplies sufficient current, up to 20 mA, at a stable voltage level, which a battery alone would not provide.

The modifications above effectively isolate the potentiostat, but further work is needed to address the incoming and outgoing analog signals. Typically, the potentiostat supplies and reads two analog voltages: an incoming applied potential waveform, e.g., triangular waveform for cyclic voltammetry, and a voltage which is proportional to the faradaic current, iR where i is the WE current and R is the resistance of the current follower resistor. Both of these voltages are traditionally applied

and measured with respect to earth ground or a virtual ground that is actively maintained in close proximity to earth ground by a negative-feedback OA circuit loop. Since the potentiostat is no longer referenced to earth ground, the circuitry must be isolated from earth ground. This is accomplished through optical isolation with four optocoupler circuits, OC1–OC4 in Figure 1B. The optocouplers transmit analog signals from an LED to a photodiode. Using two optocoupler circuits in conjunction with the battery-based power supply effectively decouples the potentiostat completely from earth ground. A similar approach has been used to amplify electrochemical reactions by coupling the electrochemical measurement to LEDs.^{29–31} The complete circuit allows the WE, CE, and RE to be placed in an external electric field and to control electrochemical reactions at arbitrary local voltages and fields. Critical to this measurement approach is that electrochemical reactions are driven by local potential differences across the WE–solution interface, rather than absolute potential with respect to earth ground, a fact that has been abundantly demonstrated in bipolar electrochemistry.

Cyclic Voltammetry in High Voltage Electric Fields.

Cyclic voltammetry was performed with a solution of 5 mM $K_3[Fe(CN)_6]$ in a pH 6.9, 100 mM phosphate buffer under active potential control in electrified fluids with external voltages ranging from 0 to 3000 V, as shown in Figure 2. The buffer pH was chosen to minimize electroosmotic flow in order to simplify interpretation of the results. The effects of the external voltage field are minimal as illustrated in Figure 2A,B. The data in Figure 2A were acquired with the WE and CE electrodes configured in a side-by-side configuration, with the WE and CE 50 and 100 μm wide, respectively, and 200 μm apart. The data in Figure 2B were acquired with the WE and CE in an opposed configuration, as shown in the inset, with 50 μm wide WE and CE, 50 μm apart. The electrode cell was placed approximately in the middle of the 1 cm long microchannel, although the electrochemical response was determined to be independent of its position along the channel. These experiments show that voltammetry can be successfully performed while the three electrode cell is in a large electric field. In both configurations, the highest external potentials reached were limited by electrical breakdown, not by any limitation imposed by the potentiostat. We hypothesize that, with more careful design of the connections, the instrument could function at local potentials up to 5 kV, which is the breakdown voltage of the isolation circuitry. In the case of in-line electrodes, Figure 2A, only minor shifts (≤ 50 mV) in the half wave potential are observed, while no shifts at all are observed in the opposed configuration explored in Figure 2B. The slightly larger than normal peak separation, ΔE_p , is likely due to the distance between WE and RE, which is much larger than the distance between WE and CE. The slight difference in performance is likely due to the geometry of the cell, particularly having WE and CE directly opposed keeps both at the same local potential. In addition, placing the Ag/AgCl RE directly above the WE and CE by using a small access hole also keeps the RE at the same local potential. This eliminates the larger shifts in half-wave potential that are typically observed with electrochemical detection in microchip capillary electrophoresis using the end-channel configuration, where increasing shifts in half-wave potential are observed as the WE is moved further into the channel. Thus, by eliminating the need to place the WE at the end of the channel and RE/CE in the grounded well, a large number of previously untenable device designs are accessible.

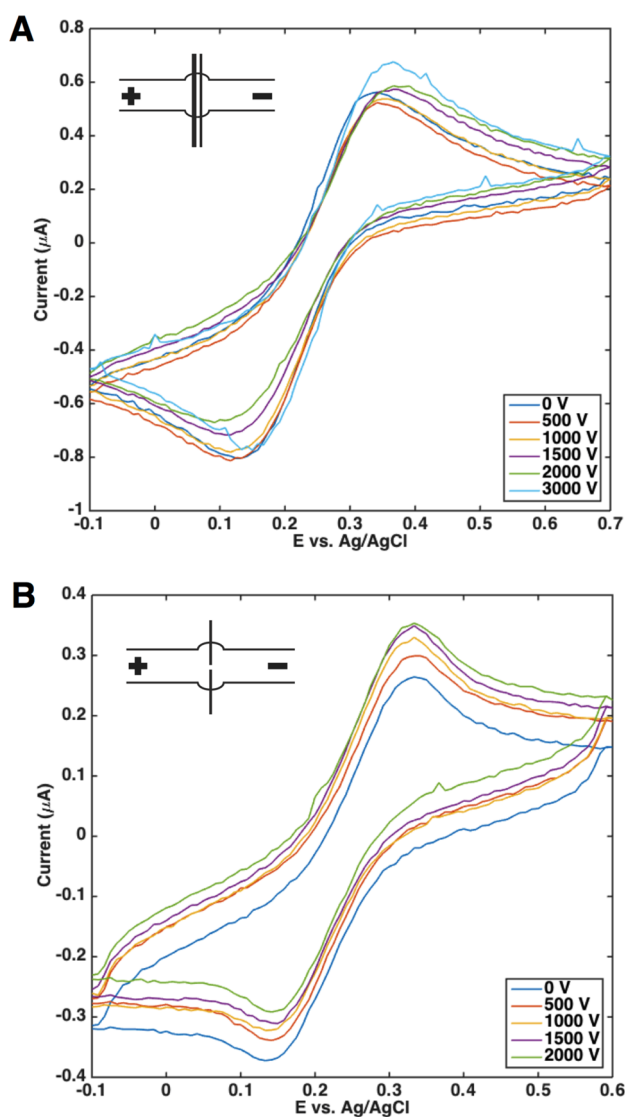


Figure 2. Cyclic voltammograms obtained from 5 mM $K_3[Fe(CN)_6]$ in 100 mM phosphate buffer at pH 6.9 with externally applied voltages ranging from 0 to 3000 V. (A) 1 cm channel with parallel WE and CE. (B) 1.2 cm length channel with opposing WE and CE. In both cases, a Ag/AgCl reference electrode is placed in a 660 μm diameter well above the CE and WE. (Insets) Schematic illustration of the WE and CE relative positions.

CONCLUSIONS

Optically isolating a potentiostat by allowing the virtual ground to float to the local potential of the reference electrode makes it possible to obtain well-behaved voltammetry at local potentials approaching 1500 V and at field strengths up to 3000 V/cm. Furthermore, this is accomplished with a true reference electrode without large shifts in the apparent reduction potential. At the price of a small increase in the complexity of the instrumentation, the performance characteristics of electrochemical detection in microchip and capillary electrophoresis are greatly extended, making it possible to incorporate electrochemical detection with electrokinetic flow-based lab-on-a-chip devices in a large number of possible device configurations.

AUTHOR INFORMATION

Corresponding Author

*E-mail: pbohn@nd.edu.

Notes

The authors declare no competing financial interest.

ACKNOWLEDGMENTS

This work was supported by the National Science Foundation through Grant 1404744 (L.P.Z.), the Department of Energy Office of Science through Grant DE FG02 07ER15851 (W.R.A.W.), and the Defense Advanced Research Projects Agency (G.M.C.). L.P.Z. acknowledges the Advanced Diagnostic and Therapeutics Initiative Fellowship. The authors thank Dr. C. Ma for useful discussions. Fabrication and structural characterization of the devices studied here were accomplished at the Notre Dame Nanofabrication Facility whose generous support is gratefully acknowledged.

REFERENCES

- (1) Kovarik, M. L.; Jacobson, S. C. *Anal. Chem.* **2009**, *81*, 7133–7140.
- (2) Piruska, A.; Gong, M.; Sweedler, J. V.; Bohn, P. W. *Chem. Soc. Rev.* **2010**, *39*, 1060–1072.
- (3) Gatimu, E. N.; Sweedler, J. V.; Bohn, P. W. *Analyst* **2006**, *131*, 705–709.
- (4) Gencoglu, A.; Minerick, A. R. *Microfluid. Nanofluid.* **2014**, *17*, 781–807.
- (5) Nyholm, L. *Analyst* **2005**, *130*, 599–605.
- (6) Rice, C. L.; Whitehead, R. *J. Phys. Chem.* **1965**, *69*, 4017–4024.
- (7) Sparreboom, W.; van den Berg, A.; Eijkel, J. C. T. *Nat. Nanotechnol.* **2009**, *4*, 713–720.
- (8) Tamaki, E.; Hibara, A.; Kim, H. B.; Tokeshi, M.; Kitamori, T. *J. Chromatogr. A* **2006**, *1137*, 256–262.
- (9) Kemery, P. J.; Steehler, J. K.; Bohn, P. W. *Langmuir* **1998**, *14*, 2884–2889.
- (10) Piruska, A.; Branagan, S. P.; Minnis, A. B.; Wang, Z.; Cropek, D. M.; Sweedler, J. V.; Bohn, P. W. *Lab Chip* **2010**, *10*, 1237–1244.
- (11) Haywood, D. G.; Harms, Z. D.; Jacobson, S. C. *Anal. Chem.* **2014**, *86*, 11174–11180.
- (12) Chang, B. Y.; Mavre, F.; Chow, K. F.; Crooks, J. A.; Crooks, R. M. *Anal. Chem.* **2010**, *82*, 5317–5322.
- (13) Chow, K. F.; Mavre, F.; Crooks, J. A.; Chang, B. Y.; Crooks, R. M. *J. Am. Chem. Soc.* **2009**, *131*, 8364.
- (14) Mavre, F.; Anand, R. K.; Laws, D. R.; Chow, K. F.; Chang, B. Y.; Crooks, J. A.; Crooks, R. M. *Anal. Chem.* **2010**, *82*, 8766–8774.
- (15) Fosdick, S. E.; Berglund, S. P.; Mullins, C. B.; Crooks, R. M. *ACS Catal.* **2014**, *4*, 1332–1339.
- (16) Perdue, R. K.; Laws, D. R.; Hlushkou, D.; Tallarek, U.; Crooks, R. M. *Anal. Chem.* **2009**, *81*, 10149–10155.
- (17) Branagan, S. P.; Contento, N. M.; Bohn, P. W. *J. Am. Chem. Soc.* **2012**, *134*, 8617–8624.
- (18) Gibson, L. R.; Branagan, S. P.; Bohn, P. W. *Small* **2013**, *9*, 90–97.
- (19) Zaino, L. P.; Contento, N. M.; Branagan, S. P.; Bohn, P. W. *ChemElectroChem* **2014**, *1*, 1570–1576.
- (20) Lacher, N. A.; Lunte, S. M.; Martin, R. S. *Anal. Chem.* **2004**, *76*, 2482–2491.
- (21) Mecker, L. C.; Martin, R. S. *Electrophoresis* **2006**, *27*, 5032–5042.
- (22) Kang, C. M.; Joo, S.; Bae, J. H.; Kim, Y. R.; Kim, Y.; Chung, T. D. *Anal. Chem.* **2012**, *84*, 901–907.
- (23) Gunasekara, D. B.; Hulvey, M. K.; Lunte, S. M. *Electrophoresis* **2011**, *32*, 832–837.
- (24) Martin, R. S.; Ratzlaff, K. L.; Huynh, B. H.; Lunte, S. M. *Anal. Chem.* **2002**, *74*, 1136.

- (25) Forry, S. P.; Murray, J. R.; Heien, M. L. A. V.; Locascio, L. E.; Wightman, R. M. *Anal. Chem.* **2004**, *76*, 4945–4950.
- (26) Wallenborg, S. R.; Nyholm, L.; Lunte, C. E. *Anal. Chem.* **1999**, *71*, 544–549.
- (27) Contento, N. M.; Bohn, P. W. *Microfluid. Nanofluid.* **2015**, *18*, 131–140.
- (28) Bard, A. J.; Faulkner, L. R. *Electrochemical Methods: Fundamentals and Applications*, 2nd ed.; Wiley: New York, 2001.
- (29) Faulkner, L. R.; He, P.; Ingersoll, D.; Huang, H.-J.; Walsh, M. R. In *Ultramicroelectrodes*; Fleishmann, M., Pons, B. S., Rolison, D. R., Schmidt, P. P.; Eds.; Datatech: Morganton, NC, 1987; pp 225–239.
- (30) Faulkner, L. R.; Walsh, M. R.; Xu, C. In *Contemporary Electroanalytical Chemistry*; Ivaska, A., Lewenstam, A., Sara, R.; Eds.; Plenum Press: New York, 1990; pp 5–14.
- (31) Sun, L.; Crooks, R. M. *J. Electrochem. Soc.* **2005**, *152*, E371–E377.